ARTICLE

ACS chemical biology

Probing the Function of Heme Distortion in the H-NOX Family

Charles Olea, Jr.[†], Elizabeth M. Boon[‡], Patricia Pellicena[†], John Kuriyan[†,‡,§,¶], and Michael A. Marletta[†,‡,¶,*]

[†]Department of Molecular and Cell Biology, [‡]Department of Chemistry, California Institute for Quantitative Biosciences, [§]Howard Hughes Medical Institute, University of California, Berkeley, California 94720, and [¶]Division of Physical Biosciences, Lawrence Berkeley National Laboratory, Berkeley, California 94720

ABSTRACT Hemoproteins carry out diverse functions utilizing a wide range of chemical reactivity while employing the same heme prosthetic group. It is clear from high-resolution crystal structures and biochemical studies that protein-bound hemes are not planar and adopt diverse conformations. The crystal structure of an H-NOX domain from *Thermoanaerobacter tengcongensis* (*Tt* H-NOX) contains the most distorted heme reported to date. In this study, *Tt* H-NOX was engineered to adopt a flatter heme by mutating proline 115, a conserved residue in the H-NOX family, to alanine. Decreasing heme distortion in *Tt* H-NOX increases affinity for oxygen and decreases the reduction potential of the heme iron. Additionally, flattening the heme is associated with significant shifts in the N-terminus of the protein. These results show a clear link between the heme conformation and *Tt* H-NOX structure and demonstrate that heme distortion is an important determinant for maintaining biochemical properties in H-NOX proteins.

The very broad range of chemistry carried out by hemoproteins has attracted a vast amount of attention for many years. Representative examples include oxygen-transporting proteins, like the globins, and potent catalysts involving high-valent iron-oxo complexes, such as the cytochrome P-450s. There are a number of factors that direct and control the type of chemistry carried out by this ubiquitous class of proteins. The coordination environment provided by the protein, for example, plays a significant role in dictating both chemistry and function. The globins have evolved to stabilize the unligated Fe(II) oxidation state and the Fe(II)$-O_2$ complex using a proximal histidine ligand. In contrast, the thiol-ligated cytochrome P450s have a stable Fe(III) oxidation state; however, when reduced to Fe(II), the iron binds O_2 and then generates a high-valent iron-oxo complex (formally the Fe(V) oxidation state). This potent oxidant is competent for hydroxylation chemistry of unactivated C$-$H bonds.

The unique and tunable chemical properties of the heme prosthetic group account for the wide range of functions observed within the hemoprotein family. The tetrapyrrole moiety of the heme is aromatic, and as such, hemes in isolation are planar. However, when protein-bound, the heme deviates significantly from planarity (*1*–*5*). Although the types of heme distortions found in hemoproteins are energetically unfavorable (*6*), they are conserved in homologous proteins from different organisms (*7*), suggesting that heme distortion is important for function. Indeed, out-of-plane heme distortions have been shown to influence the biochemical properties of both noncovalent *b*-type cytochromes, such as the globins, where the heme is bound to the protein through coordination to the iron atom of an amino acid side chain, as well as the covalent *c*-type cy-

*Corresponding author, marletta@berkeley.edu.

Received for review August 1, 2008 and accepted September 10, 2008.

Published online November 21, 2008

10.1021/cb800185h CCC: $40.75

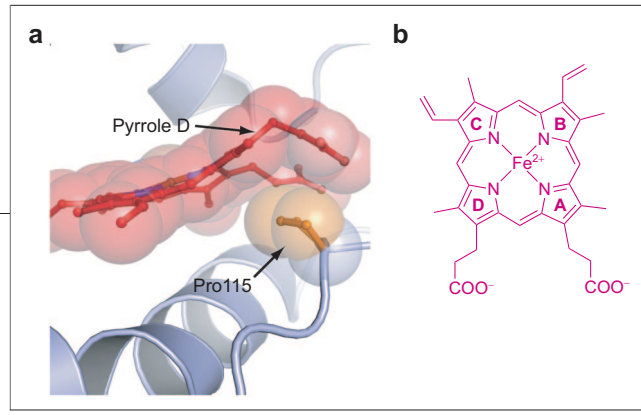

Figure 1. Heme distortion in wild-type *Tt* H-NOX. a) Ball-and-stick and space filling model of Pro115 and the surrounding heme environment of wild-type *Tt* H-NOX (*15*). The invariant Pro115 (orange) makes the largest contribution to heme (red) distortion in *Tt* H-NOX. Pro115 pushes up against pyrrole D, which causes a pronounced kink in the connected propionate group. Out-of-plane distortions of up to 2 Å are observed in *Tt* H-NOX. b) Heme prosthetic group with pyrrole groups A–D labeled.

tochromes, where a porphyrin vinyl group is attached to a protein cysteine residue by a thiol-ether linkage. For example, heme distortion affects the reduction potential (*4, 8, 9*), as well as ligand binding (*3, 10, 11*) and spectroscopic characteristics, of cytochrome *c* and model porphyrins (*12, 13*). Heme distortion also influences the mechanism of the "on/off" state in heme sensor proteins, such as FixL (*14*) and the nitrophorins (*11*), both *b*-type heme proteins.

Heme distortion and its functional outcomes are complicated. Past work has explored the environment within the pocket and the residues surrounding the bound heme; however, the role of distortion has been experimentally difficult to approach. Fortunately, the highly distorted heme in the Heme Nitric oxide/OXygen binding (H-NOX) domain from *Thermoanaerobacter tencongenesis* (*Tt* H-NOX) now provides a direct opportunity to address the importance and biochemical properties of heme nonplanarity.

The crystal structure of *Tt* H-NOX contains the most distorted heme observed to date (*15*). In eukaryotes, H-NOX domains are found as a domain within soluble guanylate cyclase (sGC) as the receptor for nitric oxide (NO) in signaling during vasodilation and neurotransmission (*16*). In prokaryotes, H-NOX proteins appear to fall into one of two classes. One type is a stand-alone protein most often found in a predicted operon with a histidine kinase and less frequently with GGDEF-diguanylate cyclase domain. The other class is fused to methyl-accepting chemotaxis domains in the same open reading frame (*17–19*). Homology to sGC as well as genomic placement suggests that H-NOX domains in prokaryotes are likely to serve as sensors for gases such as O_2 and NO. Recent results with the H-NOX from the facultative aerobe, *Shewanella oneidensis*, are consistent with this hypothesis (*19*).

The out-of-plane heme distortions found in *Tt* H-NOX show large deviations (over 2 Å) from planarity. This distortion appears to be caused by van der Waals interactions in the heme cavity, with residue Pro115 making the largest contribution (Figure 1). Pro115 is within van der Waals contact with pyrrole-D of the heme, causing the pyrrole to shift out of plane, generating a large kink in the heme propionate group. Multiple sequence alignments show that Pro115 is invariant among all H-NOX proteins, suggesting that heme distortion is conserved across the entire family. This idea has recently been substantiated as heme distortion is also observed in the crystal structures of *Nostoc* cyanobacteria H-NOX (*Ns* H-NOX) (*20*). Importantly, the same *Tt* H-NOX proline/heme interaction is maintained in *Ns* H-NOX, supporting the idea that heme distortion is universal to all H-NOX proteins.

The *Tt* H-NOX crystal structure contains two molecules in the unit cell, and one heme (molecule B) is slightly flattened compared to the other (molecule A). The degree of heme distortion is coupled to an N-terminal rotation in the wild-type structure (*15*). In this work, to directly investigate heme flattening, Pro115 has been mutated to an alanine in *Tt* H-NOX, a mutation that should allow the heme to become less distorted and, if successful, will allow for the determination of the effects of distortion on both structure and properties. Results obtained show that the heme in P115A is significantly flattened. Additionally, the mutation increases the affinity for oxygen and, in contrast to earlier studies with other hemoproteins (*10, 21*), decreases the reduction potential of the heme. Finally, a flatter heme in this mutant is correlated to a protein conformational change at the N-terminus where shifts of over 4.9 Å are observed.

RESULTS AND DISCUSSION

Design of a Planar Heme in *Tt* H-NOX. Guided by visual inspection of the structure of wild-type *Tt* H-NOX as well as energy minimizations (*15*) that predict Pro115 to contribute significantly to heme distortion, the P115A mutant was made. P115A was designed to replace the steric bulk of the cyclic three-carbon chain with a less bulky methyl group.

Structure Determination and Analysis of P115A. The crystal structure of the P115A *Tt* H-NOX domain was solved by molecular replacement and refined to 2.12 Å resolution with a final R_{work} value of 20.5% and an R_{free}

value of 25.2% (Figure 2). A total of four Fe(II)−O_2 P115A molecules (molecules A−D) were built in a monoclinic asymmetric unit cell. Crystallographic data and refinement statistics are summarized in Table 1.

Root mean square (rms) deviation from planarity, normal-coordinate analysis, and interpyrrole angles were calculated for all hemes in P115A (Supplementary Tables S1 and S2). The N-terminal and overall rms deviation from wild-type *Tt* H-NOX were calculated for P115A (Supplementary Table S3). Matrix plots based on the differences in α-carbon distances were calculated with the program DDMP (Center for Structural Biology at Yale University, New Haven, CT and Supplementary Figures S1a−S1d). These plots show that the C-terminal region overlays well with wild-type, and consequently residues 1−83 were used to calculate N-terminal rms deviation. The iron-histidine tilt was calculated using the least-squares plane of the four pyrrole nitrogens in the heme (the other atoms in the macrocycle were excluded because of the high degree of distortion) and the five imidazole ring atoms of His102 using MOLEMAN2 (*22*).

Heme Distortion in P115A *versus* Wild-Type. All four molecules in the unit cell have hemes flatter than that of wild-type *Tt* H-NOX. Molecules C and D (Figure 3) show the most significant change from wild-type (Supplementary Tables S1, S2 and S3). However, the heme atoms in molecule C have relatively high B-factor values that range from 49 to 78 Å^2. Therefore, further analysis is primarily focused on molecule D, which can be analyzed with higher certainty with B-factor values that range from 39 to 61 Å^2. Molecule A of the wild-type *Tt* H-NOX is used for comparison because it has the highest degree of heme distortion.

A comparison of P115A molecule D and wild-type *Tt* H-NOX molecule A is shown in Figure 2. The rms deviation from planarity in P115A has decreased significantly, approximately 3-fold compared to wild-type. Specifically, the rms deviation from planarity is 0.147 Å in P115A compared to 0.460 Å in the wild-type *Tt* H-NOX. The decrease in rms deviation from planarity in P115A from the most distorted heme in wild-type *Tt* H-NOX is approximately 3-fold.

Supplementary Table S1 shows the major contributions to heme distortion in P115A and wild-type *Tt* H-NOX as calculated by normal-coordinate structural analysis (*7, 23*). The major contributors to heme distortion in wild-type *Tt* H-NOX are saddling and ruffling. In all four P115A molecules (A−D), the degree of both saddling and ruffling decreases with respect to all molecules of wild-type. For example, saddling and ruffling in P115A molecule D are 0.066 Å and −0.517 Å, respectively, while in wild-type molecule A they are −1.069 Å and −1.105 Å. The angles between the planes of the pyrrole rings within the heme in P115A decrease from that in the wild-type *Tt* H-NOX (Supplementary Table S2). The pyrrole angles in molecule D range from 0° to 15°, whereas in the wild-type *Tt* H-NOX they range from 10° to 33°.

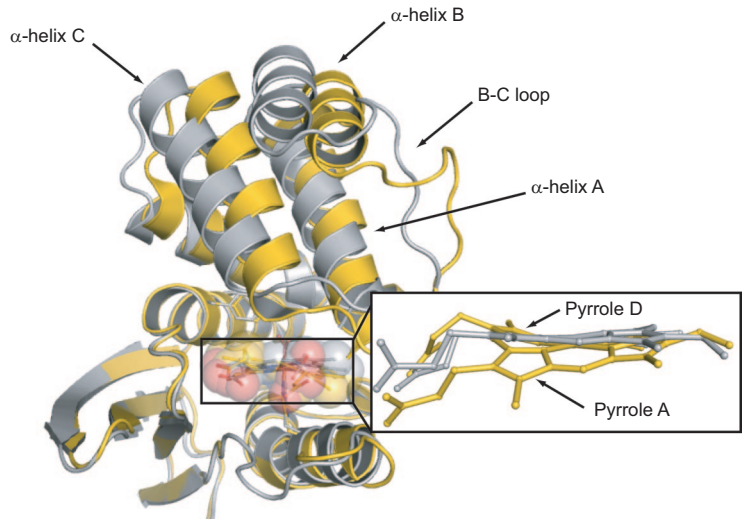

Figure 2. Structural comparison of P115A with wild-type *Tt* H-NOX. The heme in P115A (silver) is flatter than wild-type (gold). Significant translations are observed in the N-terminal region of the heme-flattened P115A crystal structure. Shown are molecule A from the monoclinic crystal structure of *Tt* wild-type H-NOX and molecule D from the P115A crystal structure.

Overall, the P115A crystal structure shows that removal of the bulky and conformationally constrained proline leads to a general flattening of the heme, as demonstrated by the decrease in all interpyrrole angles as well as decreased saddling and ruffling displacements, described above. This occurs because the pyrrole D ring and the associated propionate side chain move back into the porphyrin plane, resulting in more space in the heme pocket and allowing the heme to adopt a lower energy conformation. Therefore, the P115A structure illustrates the importance of Pro115 in maintaining the unusual deviation from planarity of the heme in *Tt* H-NOX. Because it is invariant across the entire H-NOX family, these results suggest that this residue maintains heme deformation throughout the family.

TABLE 1. Crystallographic data collection and refinement statistics

Data Collection	
Space group	*C*2
Cell dimensions	
a, *b*, *c* (Å)	116.3, 124.7, 83.6
β (deg)	126.6
Resolution (Å)	50−2.12 (2.20−2.12)
R_{merge} (%)	5.5 (45.5)
I/σ^a	20.9 (2.7)
Completeness (%)	99.2 (99.0)
Redundancy	4.3 (3.6)
Refinement	
No. of reflections	53135
$R_{work}/R_{free}{}^b$ (%)	20.5/25.2
No. atoms	
Protein	6577
Heme	172
O_2 Molecules	4
Water molecules	176
Overall *B*-factors (Å^2)	49
Root mean square deviation from ideality	
Bond lengths (Å)	0.008
Bond angles (deg)	0.898

[a]The values in parentheses relate to highest-resolution shells. [b]R_{free} is calculated for a randomly chosen 5% of reflections.

Heme Flattening Is Associated with a Movement of the N-Terminus in H-NOX. It was postulated that the degree of heme distortion would be coupled to the conformation of the wild-type structure. Difference distance matrix plots show that the C-terminus in P115A aligns well with wild-type (Supplementary Figures S1a−S1d). A plot of heme distortion *versus* N-terminal movement in P115A (Figure 3) shows a clear trend between heme distortion and N-terminal movement. A significant conformational change is observed in P115A, especially in molecule D, as compared with wild-type *Tt* H-NOX molecule A (Figure 2 and Supplementary Table S3). The N-terminal rms deviation between wild-type molecule A and P115A molecule D is 3.76 Å.

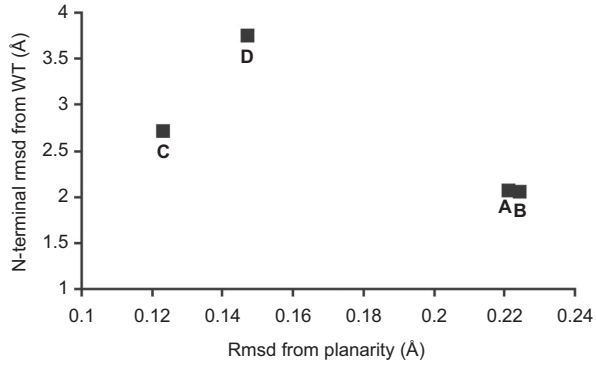

Figure 3. N-Terminal movement from wild-type *Tt* H-NOX (WT) *versus* heme distortion in P115A. The N-terminal (residues 1−83) rms deviation (Å) was calculated and plotted *versus* rms deviation (Å) from planarity for each of the four molecules in the asymmetric unit cell (A−D). Wild-type molecule A in the monoclinic space group was used for analysis.

Upon heme flattening, the tight network of van der Waals interactions in the heme pocket is lost. In particular, residues Ile5 and Met1, both on α-helix A, which are in direct contact with heme pyrrole A and the attached propionate side chain, respectively, undergo significant movement upon heme flattening. Figure 4 shows the P115A heme methyl group connected to pyrrole A moving into the plane, causing Ile5, which is part of α-helix A, to shift away from the heme. Also upon heme flattening, the propionate side chain connected to pyrrole A pushes Met1 away from the heme and the C-terminal region.

The major conformational shifts observed in P115A molecule D are localized to N-terminal α-helices A−D and the loop in between helices B and C (residues 32−45 or loop B−C) (Figure 2). As described in more detail above, α-helix A (residues 1−17) moves in conjunction with pyrrole A shifting back into plane. α-Helix C (residues 45−59) and loop B−C move along with α-helix A away from the heme and the C-terminal region. The most significant change observed in P115A can be seen in α-helix B (residues 19−29), which makes direct contact with helices A and C (Figure 2). Shifts over 4.9 Å in α-helix B are observed.

The conformation of the protein is intimately tied to the heme conformation. The large deviation in heme conformation from that of wild-type is caused by the loss of the tight network of van der Waals interactions in the heme pocket. Loss of local contacts with the heme due to heme flattening, especially at the distal pocket, results in N-terminal shifts that significantly alter the conformation of the protein. Clearly, the heme and the local protein environment are working in concert to maintain a particular conformational state in *Tt* H-NOX.

The molecular surface changes that occur upon heme flattening is a likely mechanism involved in signal transduction in this H-NOX domain. The *Tt* H-NOX domain is a member of the Tar4 family of receptors and is fused to a predicted methyl-accepting chemotaxis protein (MCP) with two predicted membrane spanning regions between these two domains. A model based on these domains places the H-NOX domain on the same side of the membrane as the MCP, suggesting that intermolecular contacts between the sensor H-NOX and the MCP are in-

volved in the signal transduction mechanism. Thus, ligand-induced H-NOX conformational changes may control methylation of the MCP. Whether heme flattening contributes to the control of methylation has yet to be evaluated.

Higher Affinity for O_2 in P115A Is Caused by Proximal Effects at the Heme. It is expected that changes in heme structure will have influence on ligand binding affinity and other heme chemical and physical properties. To evaluate the effects of heme flattening on ligand binding of *Tt* H-NOX, O_2 binding kinetics were measured and compared to those of the wild-type H-NOX. The association and dissociation rates were measured as previously described for the wild-type *Tt* H-NOX (*24*) (Supplementary Table S4). The dissociation rate of P115A was 0.22 ± 0.01 s^{-1}, compared to 1.22 ± 0.09 s^{-1} for the wild-type *Tt* H-NOX. No significant change was observed in the P115A association rate (10.4 ± 1.1 and 13.6 ± 1.0 μM^{-1} s^{-1} for P115A and wild-type, respectively), resulting in a protein with a higher affinity for O_2 (K_D is 21.2 ± 2.1 and 89.7 ± 6.2 nM for P115A and wild-type, respectively). Factors such as the distal pocket H-bonding network in *Tt* H-NOX (*24*) and the strength of the Fe-His bonds are known to contribute to higher affinity for oxygen in hemoproteins (*25, 26*). Surprisingly, all Fe-His bond lengths and distal hydrogen bonds to O_2 in P115A are within error to those of the wild-type structure (data not shown), therefore some other factor must play a role in O_2 affinity.

The Fe-histidine tilt, which has also been shown to affect ligand affinity in hemoproteins (*27*), decreased in P115A compared to wild-type (Supplementary Table S1 and Figure 5). Wild-type *Tt* H-NOX molecule A has a tilt of 78°, whereas the tilt in P115A molecule D is nearly perpendicular with a tilt of 87° (Figure 5). It is likely that flattening the heme in P115A allows for optimized bond overlap between the proximal histidine and iron, thus creating a stronger proximal bond that stabilizes the Fe(II)−O_2 complex and may explain the slower off-rate of O_2 in P115A.

We have speculated that *Tt* H-NOX serves as an oxygen sensor for the obligate anaerobe *T. tengcongensis* based on the fact that O_2 binding to this H-NOX is very tight (K_D = 90 nM). The fold of *Tt* H-NOX may tune the affinity for oxygen by distorting the heme so that the K_D is set for the appropriate physiological response. The situation may not be this simple, however. Taylor and colleagues (*28*) showed that *Desulfovibrio vulgaris* Hildenborough, a sulfate-reducing bacterium thought to be an obligate anaerobe, actually preferred an oxygen concentration of 0.02−0.04% (0.24−0.48 μM). This O_2 concentration was also shown to support growth. Hence, sensors for O_2 are likely tuned to respond to changing environmental conditions and complex physiological responses.

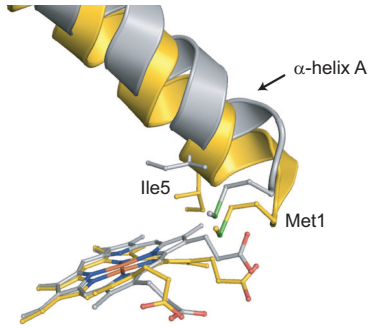

Figure 4. The effect of heme flattening on the N-terminal domain. Shown is a comparison of P115A molecule D (silver) and wild-type monoclinic *Tt* H-NOX molecule A (gold) heme/N-terminal interface. The planar heme makes new contacts with Met1 and Ile5 of α-helix A, which shifts the helix away from the C-terminal domain. Shifting of α-helix A, along with the rest of the N-terminal region, causes shifts over 4.9 Å.

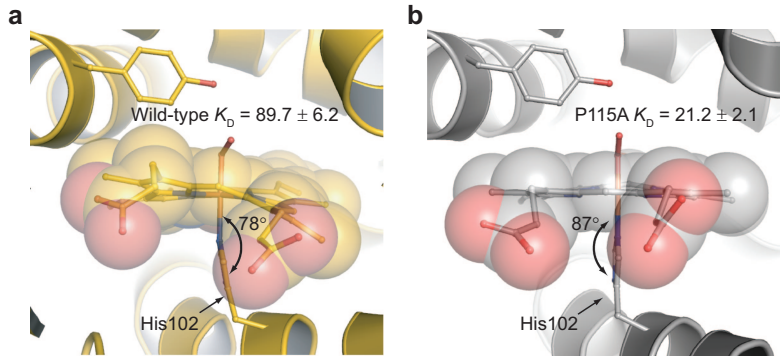

Figure 5. Comparison of the iron−histidine bond geometry. Shown are the iron−histidine tilts of a) wild-type *Tt* H-NOX (gold) and b) P115A (silver). The least-squares plane of the heme was calculated using the four pyrrole nitrogens of the heme (other atoms were excluded because of the high degree of distortion) and the five imidazole ring atoms of His102 using MOLEMAN2 (*22*). Wild-type has a tilt of 78°, whereas P115A has a tilt of 87°.

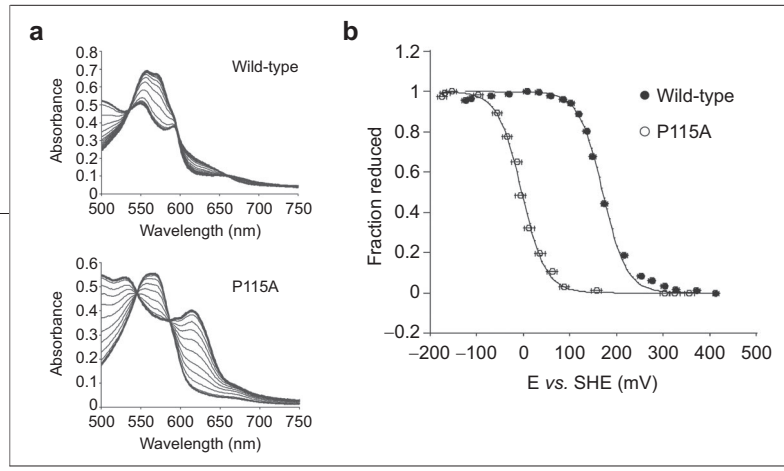

Figure 6. Reduction potential of wild-type *Tt* H-NOX and P115A. a) Titration spectra for wild-type *Tt* H-NOX and P115A. b) Titration curves for wild-type *Tt* H-NOX and P115A. The reduction potentials of P115A and wild-type *Tt* H-NOX were determined against the standard hydrogen electrode (SHE). The ratio of reduced Fe^{2+} to oxidized Fe^{3+} heme was measured on the basis of their α/β maximum at approximately 557 nm for wild-type. The difference in absorbance of the α/β maximum for reduced and the α/β minimum for oxidized was used to calculate the fraction reduced for P115A. The voltage against the SHE was measured for both oxidative and reductive titrations of wild-type and P115A. Error bars represent the standard error.

Reduction Potential Decreases in P115A. To determine whether chemical properties of the heme are sensitive to heme conformation, the reduction potential was measured for P115A and *Tt* H-NOX. P115A has a reduction potential significantly lower than that of wild-type. The reduction potentials of P115A and wild-type *Tt* H-NOX are -3.8 ± 10.2 and 167.0 ± 6.7 mV *versus* the standard hydrogen electrode (SHE) (Figure 6), respectively.

Previous studies have suggested that factors such as electrostatic interactions near the heme pocket control hemoprotein reduction potentials (*29–32*). In particular, it has been demonstrated that the reduction potential increases as a function of decreasing dielectric constant (*33, 34*); however, we cannot definitively comment on a change in the dielectric environment in P115A *versus* the wild-type protein. While the P115A mutant was designed to specifically address the role of heme distortion, the mutation could introduce other changes such as an alteration in the dielectric of the heme environment.

Implications for the Role of Heme Distortion in H-NOX Proteins. Our results show that (i) Pro115 is important for maintaining heme distortion in *Tt* H-NOX, (ii) heme distortion maintains a particular molecular oxygen K_D and a particular heme iron reduction potential, presumably at their physiologically relevant values, and (iii) heme distortion is correlated with movement in the N-terminal region of the *Tt* H-NOX. Thus, the heme and the surrounding environment work in conjunction to maintain conformation and function in *Tt* H-NOX.

As noted by Shelnutt and colleagues (*1*), porphyrin deformations are often conserved within functional classes of proteins, strongly supporting the idea that these deformations are important for function. Pro115 is likely to be important for the function of the H-NOX family since it is conserved in the entire class of proteins. Heme distortion in *Tt* H-NOX is essential for maintaining its structural conformation and biochemical properties. The data show that heme distortion contributes to maintaining a specific K_D for oxygen and reduction potential of the heme iron. Additionally, heme distortion is related to the conformation of *Tt* H-NOX. The heme and the surrounding environment work in concert to maintain a particular conformation and fold.

Conclusions. The influence of heme distortion on function has been a long-standing question and certainly related to the diverse chemistry exhibited by this large class of proteins. While many structural and biochemical studies over the past several decades have made note of heme distortion, a systematic approach has not appeared. The challenge is to trap the heme in different conformations under similar conditions (pH, salinity, temperature, etc.) and ligation state. The H-NOX family, for the reasons outlined above, provides the opportunity to carry out such an investigation, and the first step in this regard is reported here. As discussed, heme distortion in the nitrophorins is significant (*9, 11*). Walker and colleagues (*10*) attempted to trap a flattened heme in nitrophorin 2. They speculated that distal pocket mutations in the protein would flatten the heme and speculated further about a change in redox potential. However, very little change in heme conformation was observed between the hemes of both the wild-type protein and the mutant crystal structures (PDB codes 2A3F and 2ALL). The H-NOX results presented in this paper show a heme trapped in different conformational states generated by a single point mutation. The differences in ligand binding and redox potential correlate with the changes in heme distortion; however, our results do not agree with a previous report that shows an opposite trend in heme ruffling *versus* redox potential in cytochromes c_3 (*21*). Clearly, the redox potential and ligand binding will depend on multiple factors in-

cluding the heme environment, ligands to the iron and covalent *versus* noncovalent heme, as well as the degree of heme distortion. The large movement of the N-terminal region of the protein was unexpected and provides a clear example of protein conformation linked to the heme cofactor. The movement was presaged by what we previously observed in molecules A and B in our first structure (*15*); however, it was uncertain whether the heme conformation and N-terminal shift were an outcome of the crystallization. Our results here unambiguously show the importance of heme conformation in protein structure and chemistry.

METHODS

Expression of P115A Mutant of *Tt* H-NOX in *E. coli*. Mutagenesis was carried out using the QuikChange protocol from Stratagene. Cell culture procedures and purification of P115A for kinetics were carried out as previously described (*18*). Cell culture and expression procedures for P115A crystallization and redox potentiometry were carried out as described above with the exception that the growth media was Terrific Broth.

Purification of P115A for Crystallization. Cell lysis and thermal treatment were carried out as previously described (*18*). The supernatant after thermal treatment was concentrated to 10 mL using a Vivaspin concentrator (Sartorius, 10 kDa) and loaded onto a Superdex 200 HiLoad 26/60 gel filtration column (Pharmacia) that was equilibrated with buffer A (50 mM TEA, pH 7.5, 50 mM NaCl, and 5% glycerol) at a flow rate of 0.5 mL min^{-1}. Fractions containing P115A were pooled on the basis of the intensity of the red/brown color and applied to a POROS HQ 7.9 mL (1 × 10 cm, 10 μm) anion-exchange column (Applied Biosystems) that had been equilibrated with buffer A. The flow rate was 10 mL min^{-1}, and the flow-through was collected. Aliquots (2 mL) of P115A were then loaded onto a Superdex 75 HiLoad 26/60 gel filtration column (Pharmacia) that was equilibrated with buffer A at a flow rate of 0.5 mL min^{-1}. P115A was isolated as the Fe(II)−O_2 complex (*18*) and stored at −80 °C.

Crystallization of *Tt* P115A. Samples of P115A were equilibrated with 20 mM TEA (pH 7.5) and concentrated to 30 mg mL^{-1}. Crystals were grown by hanging drop vapor diffusion by mixing 1 μL of the protein solution with 1 μL of the reservoir solution and equilibrating against a 750 μL reservoir of 0.1 M NaSCN, 0.1 M Tris (pH 9.1), 0.2 M $(NH_4)_2(SO_4)$, and 18% (w/v) PEG 8000 at 16 °C. Crystals began to appear within 24 h. Cryoprotection was achieved by transferring the crystals stepwise into mother liquor solutions containing 10% and 15% glycerol and ending with 20% glycerol and 5% xylitol. Crystals of P115A were obtained in the *C*2 space group, flash frozen in liquid propane, and stored in liquid nitrogen.

X-ray Data Collection, Phasing and Refinement. X-ray data were collected by using synchrotron radiation at beamline 8.2.1 at the Advanced Light Source, Lawrence Berkeley National Laboratory. Diffraction images were collected at 100 K with 10 s exposure time and 1° oscillations per frame. Data were processed with the HKL2000 suite (*35*). Molecular replacement was carried out with Phaser (*36*) using wild-type H-NOX (PDB ID 1U55) as a search model. Model building was carried out by using the programs O (*37*) and Coot (*38*). Refinement was carried out by using CNS (*39*) and Phenix (*40*) with TLS refinement parameters incorporated. The final model includes four P115A molecules in the asymmetric unit. The structure of P115A was refined to a final R_{work} of 20.5% (R_{free} = 25.2%) at 2.12 Å.

Kinetics. The on-rate of O_2 binding to heme and dissociation of O_2 from heme were measured as previously described (*24*).

Redox Potentiometry. Potentiometric titrations were performed as previously described (*41*). The change in the Fe oxidation state in *Tt* H-NOX was monitored by the absorbance change at α/β region maximum (~557 nm). For P115A the oxidation state change was measured by the difference of absorbance of the α/β maximum of the oxidized and the α/β minimum of the reduced oxidation state spectra.

Accession Codes: The atomic coordinates have been deposited in the Protein Data Bank, www.pdb.org (PDB ID 3EEE; RCSB ID code rcsb049218).

Acknowledgment: This work was supported by the National Institutes of Health grant GM070671 and a Eugene Cota-Robles Fellowship to C.O. We are grateful to Debora Makino, Meindert Lamers, Xeuwu Zhang, Nick Levinson, and members of the Kuriyan laboratory for assistance and advice during structure refinement. We thank Wendy Belliston-Bittner, Jay Winkler, and Harry Gray at the Beckman Institute Laser Resource Center at the California Institute of Technology for their essential help in measuring oxygen association rates. We thank Katelyn Connell and Matthew Volgraf for initial studies with the P115A mutant. We thank members of the M.A.M. and J.K. laboratories for helpful discussions and review of the manuscript. We also thank Mark Hargrove (University of Iowa) for instruction on redox potential measurements.

Supporting Information Available: This material is available free of charge *via* the Internet.

REFERENCES

1. Shelnutt, J. A., Song, X. Z., Ma, J. G., Jia, S. L., Jentzen, W., and Medforth, C. J. (1998) Nonplanar porphyrins and their significance in proteins, *Chem. Soc. Rev. 27*, 31–41.
2. Zbylut, S. D., and Kincaid, J. R. (2002) Resonance Raman evidence for protein-induced out-of-plane distortion of the heme prosthetic group of mammalian lactoperoxidase, *J. Am. Chem. Soc. 124*, 6751–6758.
3. Li, D., Stuehr, D. J., Yeh, S. R., and Rousseau, D. L. (2004) Heme distortion modulated by ligand-protein interactions in inducible nitric oxide synthase, *J. Biol. Chem. 279*, 26489–26499.
4. Ravikanth, M., and Chandrashekar, T. K. (1995) Nonplanar porphyrins and their biological relevance—ground and excited-state dynamics, *Coord. Chem. 82*, 105–188.
5. Weichsel, A., Andersen, J. F., Roberts, S. A., and Montfort, W. R. (2000) Nitric oxide binding to nitrophorin 4 induces complete distal pocket burial, *Nat. Struct. Biol. 7*, 551–554.
6. Anderson, K. K., Hobbs, J. D., Luo, L. A., Stanley, K. D., Quirke, J. M. E., and Shelnutt, J. A. (1993) Planar nonplanar conformational equilibrium in metal derivatives of octaethylporphyrin and *meso*-nitrooctaethylporphyrin, *J. Am. Chem. Soc. 115*, 12346–12352.
7. Jentzen, W., Ma, J. G., and Shelnutt, J. A. (1998) Conservation of the conformation of the porphyrin macrocycle in hemoproteins, *Biophys. J. 74*, 753–763.
8. Barkigia, K. M., Chantranupong, L., Smith, K. M., and Fajer, J. (1988) Structural and theoretical models of photosynthetic chromophore. Implications for redox, light-absorption properties and vectorial electron flow, *J. Am. Chem. Soc. 110*, 7566–7567.

9. Maes, E. M., Roberts, S. A., Weichsel, A., and Montfort, W. R. (2005) Ultrahigh resolution structures of nitrophorin 4: heme distortion in ferrous CO and NO complexes, *Biochemistry 44*, 12690–12699.
10. Shokhireva, T., Berry, R. E., Uno, E., Balfour, C. A., Zhang, H., and Walker, F. A. (2003) Electrochemical and NMR spectroscopic studies of distal pocket mutants of nitrophorin 2: stability, structure, and dynamics of axial ligand complexes, *Proc. Natl. Acad. Sci. U.S.A. 100*, 3778–3783.
11. Roberts, S. A., Weichsel, A., Qiu, Y., Shelnutt, J. A., Walker, F. A., and Montfort, W. R. (2001) Ligand-induced heme ruffling and bent NO geometry in ultra-high-resolution structures of nitrophorin 4, *Biochemistry 40*, 11327–11337.
12. Ma, J. G., Laberge, M., Song, X. Z., Jentzen, W., Jia, S. L., Zhang, J., Vanderkooi, J. M., and Shelnutt, J. A. (1998) Protein-induced changes in nonplanarity of the porphyrin in nickel cytochrome *c* probed by resonance Raman spectroscopy, *Biochem. 37*, 5118–5128.
13. Ryeng, H., and Ghosh, A. (2002) Do nonplanar distortions of porphyrins bring about strongly red-shifted electronic spectra? Controversy, consensus, new developments, and relevance to chelatases, *J. Am. Chem. Soc. 124*, 8099–8103.
14. Gong, W., Hao, B., Mansy, S. S., Gonzalez, G., Gilles-Gonzalez, M. A., and Chan, M. K. (1998) Structure of a biological oxygen sensor: a new mechanism for heme-driven signal transduction, *Proc. Natl. Acad. Sci. U.S.A. 95*, 15177–15182.
15. Pellicena, P., Karow, D. S., Boon, E. M., Marletta, M. A., and Kuriyan, J. (2004) Crystal structure of an oxygen-binding heme domain related to soluble guanylate cyclases, *Proc. Natl. Acad. Sci. U.S.A. 101*, 12854–12859.
16. Denninger, J. W., and Marletta, M. A. (1999) Guanylate cyclase and the •NO/cGMP signaling pathway, *Biochim. Biophys. Acta 1411*, 334–350.
17. Iyer, L. M., Anantharaman, V., and Aravind, L. (2003) Ancient conserved domains shared by animal soluble guanylyl cyclases and bacterial signaling proteins, *BMC Genomics 4*, 5.
18. Karow, D. S., Pan, D., Tran, R., Pellicena, P., Presley, A., Mathies, R. A., and Marletta, M. A. (2004) Spectroscopic characterization of the soluble guanylate cyclase-like heme domains from *Vibrio cholerae* and *Thermoanaerobacter tengcongensis*, *Biochemistry 43*, 10203–10211.
19. Price, M. S., Chao, L. Y., and Marletta, M. A. (2007) *Shewanella oneidensis* MR-1 H-NOX regulation of a histidine kinase by nitric oxide, *Biochemistry 46*, 13677–13683.
20. Ma, X., Sayed, N., Beuve, A., and van den Akker, F. (2007) NO and CO differentially activate soluble guanylyl cyclase *via* a heme pivot-bend mechanism, *EMBO J. 26*, 578–588.
21. Ma, J. G., Zhang, J., Franco, R., Jia, S. L., Moura, I., Moura, J. J., Kroneck, P. M., and Shelnutt, J. A. (1998) The structural origin of nonplanar heme distortions in tetraheme ferricytochromes c_3, *Biochemistry 37*, 12431–12442.
22. Kleywegt, G. J., and Jones, T. A. (1999) Software for handling macromolecular envelopes, *Acta Crystallogr., Sect. D: Biol. Crystallogr. 55*, 941–944.
23. Shelnutt, J. A. (2001) Normal-coordinate structural decomposition and the vibronic spectra of porphyrins, *J. Porphyrins Phthalocyanines 5*, 300–311.
24. Boon, E. M., Huang, S. H., and Marletta, M. A. (2005) A molecular basis for NO selectivity in soluble guanylate cyclase, *Nat. Chem. Biol. 1*, 53–59.
25. Giangiacomo, L., Ilari, A., Boffi, A., Morea, V., and Chiancone, E. (2005) The truncated oxygen-avid hemoglobin from *Bacillus subtilis*: X-ray structure and ligand binding properties, *J. Biol. Chem. 280*, 9192–9202.
26. Capece, L., Marti, M. A., Crespo, A., Doctorovich, F., and Estrin, D. A. (2006) Heme protein oxygen affinity regulation exerted by proximal effects, *J. Am. Chem. Soc. 128*, 12455–12461.
27. Friedman, J. M., Rousseau, D. L., Ondrias, M. R., and Stepnoski, R. A. (1982) Transient Raman study of hemoglobin: structural dependence of the iron-histidine linkage, *Science 218*, 1244–1246.
28. Johnson, M. S., Zhulin, I. B., Gapuzan, M. E., and Taylor, B. L. (1997) Oxygen-dependent growth of the obligate anaerobe *Desulfovibrio vulgaris* Hildenborough, *J. Bacteriol. 179*, 5598–5601.
29. Mauk, A. G., and Moore, G. R. (1997) Control of metalloprotein redox potentials: What does site-directed mutagenesis of hemoproteins tell us? *J. Biol. Inorg. Chem. 2*, 119–125.
30. Mao, J. J., Hauser, K., and Gunner, M. R. (2003) How cytochromes with different folds control heme redox potentials, *Biochem. 42*, 9829–9840.
31. Kennedy, M. L., Silchenko, S., Houndonougbo, N., Gibney, B. R., Dutton, P. L., Rodgers, K. R., and Benson, D. R. (2001) Model hemoprotein reduction potentials: the effects of histidine-to-iron coordination equilibrium, *J. Am. Chem. Soc. 123*, 4635–4636.
32. Kassner, R. J. (1972) Effects of nonpolar environments on the redox potentials of heme complexes, *Proc. Natl. Acad. Sci. U.S.A. 69*, 2263–2267.
33. Tezcan, F. A., Winkler, J. R., and Gray, H. B. (1998) Effects of ligation and folding on reduction potentials of heme proteins, *J. Am. Chem. Soc. 120*, 13383–13388.
34. Cowley, A. B., Kennedy, M. L., Silchenko, S., Lukat-Rodgers, G. S., Rodgers, K. R., and Benson, D. R. (2006) Insight into heme protein redox potential control and functional aspects of six-coordinate ligand-sensing heme proteins from studies of synthetic heme peptides, *Inorg. Chem. 45*, 9985–10001.
35. Otwinowski, Z., and Minor, W. (1997) Processing of X-ray diffraction data collected in oscillation mode, *Macromol. Crystallogr., Part A 276*, 307–326.
36. McCoy, A. J., Grosse-Kunstleve, R. W., Storoni, L. C., and Read, R. J. (2005) Likelihood-enhanced fast translation functions, *Acta Crystallogr., Sect. D: Biol. Crystallogr. 61*, 458–464.
37. Kleywegt, G. J., and Jones, T. A. (1996) Efficient rebuilding of protein structures, *Acta Crystallogr., Sect. D: Biol. Crystallogr. 52*, 829–832.
38. Emsley, P., and Cowtan, K. (2004) Coot: model-building tools for molecular graphics, *Acta Crystallogr., Sect. D: Biol. Crystallogr. 60*, 2126–2132.
39. Brunger, A. T., Adams, P. D., Clore, G. M., DeLano, W. L., Gros, P., Grosse-Kunstleve, R. W., Jiang, J. S., Kuszewski, J., Nilges, M., Pannu, N. S., Read, R. J., Rice, L. M., Simonson, T., and Warren, G. L. (1998) Crystallography and NMR system: a new software suite for macromolecular structure determination, *Acta Crystallogr., Sect. D: Biol. Crystallogr. 54*, 905–921.
40. Adams, P. D., Grosse-Kunstleve, R. W., Hung, L. W., Ioerger, T. R., McCoy, A. J., Moriarty, N. W., Read, R. J., Sacchettini, J. C., Sauter, N. K., and Terwilliger, T. C. (2002) PHENIX: building new software for automated crystallographic structure determination, *Acta Crystallogr., Sect. D: Biol. Crystallogr. 58*, 1948–1954.
41. Dutton, P. L. (1978) Redox potentiometry: determination of midpoint potentials of oxidation-reduction components of biological electron-transfer systems, *Methods Enzymol. 54*, 411–435.